Experimental Thermal and Fluid Science 136 (2022) 110651

Contents lists available at ScienceDirect

Experimental Thermal and Fluid Science

journal homepage: www.elsevier.com/locate/etfs

Characterization of jet parameters related to cavitation bubble dynamics in a vicinity of a flat liquid-liquid interface

Uroš Orthaber, Matevž Dular, Rok Petkovšek *

University of Ljubljana, Faculty of Mechanical Engineering, Aškerčeva 6, 1000 Ljubljana, Slovenia

ARTICLE INFO

Keywords:
Cavitation
Liquid-liquid interface
Bubble
Jet
Anisotropy parameter

ABSTRACT

Presented study analyses different jet parameters that appear during and after bubble collapse, namely bubble center displacement, length of a jet-pierced bubble and size of the rebounded bubble and their relation to anisotropy parameter in a vicinity of a liquid–liquid interface. In experiments cavitation bubble was produced with a focused pulsed laser and its dynamics was recorded by a high-speed camera. Two different types of liquid-liquid interfaces consisting of distilled water and two types of silicone oil were used for the study in order to be able to compare the influence of anisotropy parameter on the magnitude of considered jet parameters. The elongation of the cavitation bubble during jet protrusion was analysed and compared for both interface types. The study exhibits systemic approach to jet parameter consideration and presents an important step in understanding the behaviour of cavitation bubble near liquid-liquid interfaces.

1. Introduction

Cavitation remains a popular and important subject of scientific investigations due to its applicability in the fields of industry, medicine, chemistry, food processing, metallurgy, nanomaterials and many others [1–7]. Phenomena associated with cavitation play a key role in kidney stone removal surgery [8,9], membrane rupturing in ophthalmic treatments [10,11], surface cleaning [12], homogenization of colloidal liquids [13], water purification [14,15], fragmentation, de-agglomeration and dispersion of crystals [16], exfoliation of nanomaterials [17] and in emulsion preparation [18,19]. Motivation for study of cavitation also stems from the need to avoid its undesired effects, most importantly in engines that use propellers and pumps, which are susceptible to erosion related to cavitation bubbles [20–23].

The first study dealing with cavitation effects in a vicinity of a liquid–liquid interface is a paper by Chahine & Bovis [24], in which authors address the liquid jet dependence on the distance between the interface and the center of the bubble. Significant amount of work was done recently to gain deeper understanding of ultrasonic emulsification. The revitalisation of the research field was sparked by observations of Stepišnik Perdih et al. [18] who challenged the previous understanding of the emulsification process. Another step towards deeper understanding of the process was recently made by Wu et al. [19] who studied the role of the presence of gas bubbles in the process. Since only bubble clusters with a rare appearance of a single cavitation bubble can be generated by ultrasound, an even deeper insight could not be obtained in these studies. Hence we developed a technique, where laser breakdown, in either water or oil, is used to observe the interaction between a single bubble and the liquid–liquid interface [25]. In that study some questions remained open due to the curvature of the interface, which does not relate well to the applied process. In this paper we improved and substantially expanded the research presented in the previous paper. By implementing a method proposed in [26], a completely flat liquid–liquid interface was achieved without the meniscus effect taking place, which typically inhibits a detailed study of bubble dynamics. In addition to that, a large number of measurements with varying parameters were performed with a high-speed camera in order to statistically demonstrate the influence of anisotropy parameter on cavitation bubble dynamics.

Anisotropy parameter ζ was introduced by Supponen et al. [27] and represents a dimensionless measure of the liquid momentum at the collapse point. Anisotropy parameter is associated with the magnitude of different observable jet parameters, such as bubble displacement, jet speed, jet-impact time and others. In the case of liquid–liquid interface the anisotropy parameter can be expressed as:

$$\zeta = 0.195\gamma^{-2}(\rho_1 - \rho_2)(\rho_1 + \rho_2)^{-1}\mathbf{n}$$

where ρ_1 represents density of the liquid in which cavitation bubble

* Corresponding author.
E-mail address: rok.petkovsek@fs.uni-lj.si (R. Petkovšek).

https://doi.org/10.1016/j.expthermflusci.2022.110651
Received 30 January 2021; Received in revised form 18 January 2022; Accepted 21 March 2022
Available online 26 March 2022

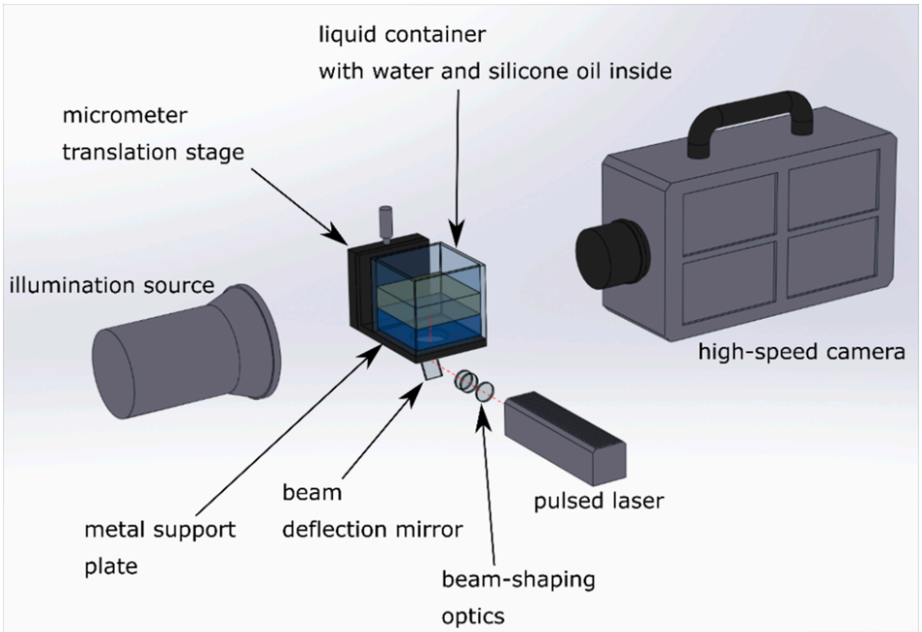

Fig. 1. Experimental setup scheme.

is generated and ρ_2 is the density of the liquid that forms interface with the first liquid, **n** is a normal unit vector on the interface pointing to the bubble center and γ is a dimensionless measure of the relative distance between the center of cavitation bubble and the interface, defined as:

$$\gamma = h/R_{max}$$

where h is a distance between the center of the bubble and the liquid–liquid interface and R_{max} is a maximum bubble radius.

Since anisotropy parameter depends on the difference in densities of both liquids, it is expected the magnitude of observable jet parameters to be different when replacing one liquid with another. For the purpose of this study two different interfaces were considered, both consisted of water on one side and silicone oil on the other. Two types of silicone oil with different densities were chosen. It is expected that the jet parameters will be more pronounced in the case where difference in densities between both liquids is higher. Three different jet parameters were selected for the study, namely bubble center displacement, length of a jet-pierced bubble and size of the rebounded bubble. Special emphasis was put on bubble dynamics in the immediate vicinity of the interface.

Table 1
Characteristics of two types of liquid-liquid interfaces used in experiments.

	interface 1		interface 2	
	liquid 1	liquid 2	liquid 1	liquid 2
substance	distilled water	silicone oil	distilled water	silicone oil
density (g/mL)	0.997	0.913	0.997	0.960
kinematic viscosity (cst)	0.89	5	0.89	50
anisotropy parameter	$\zeta_1 = 0.0086\gamma^{-2}\boldsymbol{n}$		$\zeta_2 = 0.0037\gamma^{-2}\boldsymbol{n}$	

2. Experimental setup

Experimental setup was similar to the one used in [25]. Cavitation bubble was produced by a 5 ns Q–switched Nd:YAG pulsed laser. The incident laser beam with a wavelength of 1064 nm was tightly focused and had a numerical aperture of approximately 0.25. Laser pulse energy was set to 10 mJ, which is well above the threshold for optical breakdown in water and silicone oil. A polycarbonate liquid container with dimensions 10 × 10 × 10 cm containing distilled water and silicone oil was placed on a supporting metal plate, which was attached to a vertical micrometer translation stage. The translation stage was used to control the position of a cavitation bubble and the distance between the bubble and the interface. This was possible since laser beam entered liquid container from the bottom through a hole in the supporting metal plate. High-speed camera Photron Fastcam SA-Z was used to record bubble dynamics at a frame rate of 210,000 fps. Illumination was achieved by Ryobi One + LED light source operating at 50,000 lm. Experimental setup scheme is depicted in Fig. 1.

Special attention was put to eliminate the meniscus effect from the recordings. Meniscus effect is manifested as a dark strip on the recorded frame and is a consequence of liquid wetting on the container wall. When poured in a container, the liquid surface is curved on the edges of the container due to intermolecular forces, causing the liquid to form a contact angle with respect to the container wall.

In the study presented in this paper, approach to minimize meniscus effect proposed by Tsai et al. [26] was considered. Liquid container was made of polycarbonate to reduce the static contact angle by a maximum amount. Moreover, a syringe was used to add and remove water from the tank in order to achieve near 90° dynamic contact angle. After the relaxation, the laser was triggered and recording of bubble dynamics was performed with a high speed camera.

Since anisotropy parameter is proportional to the difference of densities of liquids on each side of the interface, it is expected that jet parameters would be more or less pronounced depending on the liquids chosen for experiments. It was decided that the denser liquid will be in all cases distilled water with a density of 0.997 g/mL at 25 °C and the less dense liquid will be in first case silicone oil with a density of 0.913 g/ml and in the second case silicone oil with a density of 0.960 g/mL. Both types of silicone oil differ also in viscosity, however viscosity has a negligible effect on bubbles. According to numerous studies [27–30] influence of viscosity and surface tensions on cavitation bubble dynamics is negligible unless for extremely small bubbles with sizes less than 10^{-5} mm. Some experimental studies analysed influence of surface tension, vapour pressure and other factors on bubble dynamics, however, the bubbles were quite small and the used liquids were very different from one another [31,32]. Since the presented study deals with bubbles with a diameter of 1 mm and more it is thus justified to neglect mentioned contributions, especially since the surface tension of different

Table 2
Description of recording conditions for selected recordings.

	γ *coefficient*	Substance in which bubble is produced	Bubble position with respect to the interface
Fig. 2a	1.78	Water	Far from the interface
Fig. 2b	1.69	Silicone oil	Far from the interface
Fig. 3a	0.38	Water	Near the interface
Fig. 3b	0.44	Silicone oil	Near the interface
Fig. 4	0	Water and silicone oil	At the interface

types of silicone oils is almost the same, while vapour pressure tends to be very low. Thus, by far the most important factor in determining bubble dynamics are characteristics of the interface itself, i.e. anisotropy parameter. In Table 1 characteristics of liquids used for experiments as well as anisotropy parameter as a function of γ coefficient are listed. Coefficient γ values were varied from 0 to approximately 2 on each side of the interface. In case of interface 1 anisotropy parameter ζ_1 is more than twice the value than in case of interface 2 ($\zeta_1/\zeta_2 = 2.32$), which should influence observable jet parameters, namely bubble center displacement, length of jet–pierced bubble and size of the rebounded bubble. There was one repetition for each experiment.

3. Results and discussion

3.1. Different regimes of bubble dynamics

Frames from recordings of cavitation bubble were arranged in frame sequences to offer a comprehensive overview of the bubble dynamics in different circumstances. The first frame in the recording in which cavitation bubble appears was marked as 0 μs, the following frames are marked relatively with respect to the first frame. Although γ served as independent variable in experiments, it was actually anisotropy parameter ζ, where the focus of the study was directed. This parameter is associated with respective surface 1 or 2 and the ratio between both values is fixed, independently of γ. We are thus observing the influence of the stated anisotropy parameter ratio ($\zeta_1/\zeta_2 = 2.32$) to selected jet parameters.

Selected recording sequences shown in following figures demonstrate different examples of cavitation bubble dynamics near interface 1. In Table 2 facts about recording sequences from each figure are stated.

Examples demonstrate bubble dynamics at γ coefficient assuming values larger than 1, between 0 and 1 and approximately 0 on each side of the liquid–liquid interface. When γ is larger than 1, the bubble is furthest from the interface and the interface is expected to have least influence on its dynamics. When γ is smaller than 1, bubble maximum radius is smaller than the bubble-membrane separation distance and significant influence on bubble dynamics is expected. Likewise in case of $\gamma \approx 0$.

In Fig. 2 recording sequences of bubble dynamics at γ greater than 1 on both sides of the interface are shown. Silicone oil is on the left side of the interface and distilled water is on the right side. Both liquids appear grey in the recordings, while bubble is black. Frames are flipped by 90° relatively to the actual setup due to high-speed camera positioning. Laser beam is incident from the right on each frame. Very weak influence of cavitation bubble on the interface is noticed. The interface remains almost flat throughout the bubble oscillation cycle with only small bending during the bubble expansion phase in both cases (see frames at 114.29 μs). Liquid jet is detected by observing the elongated shape of the rebounded bubble. It appears in both cases and is always directed from left to right. The jet direction is determined by anisotropy parameter vector, which in case of liquid–liquid interface always points towards denser liquid [27].

Fig. 3 shows recording sequences of cavitation bubble dynamics near a liquid–liquid interface. Coefficient γ is in both cases less than 0.5. Very apparent bending of the interface is caused by the expanding bubble. Strong jetting is produced upon bubble collapse, due to the close

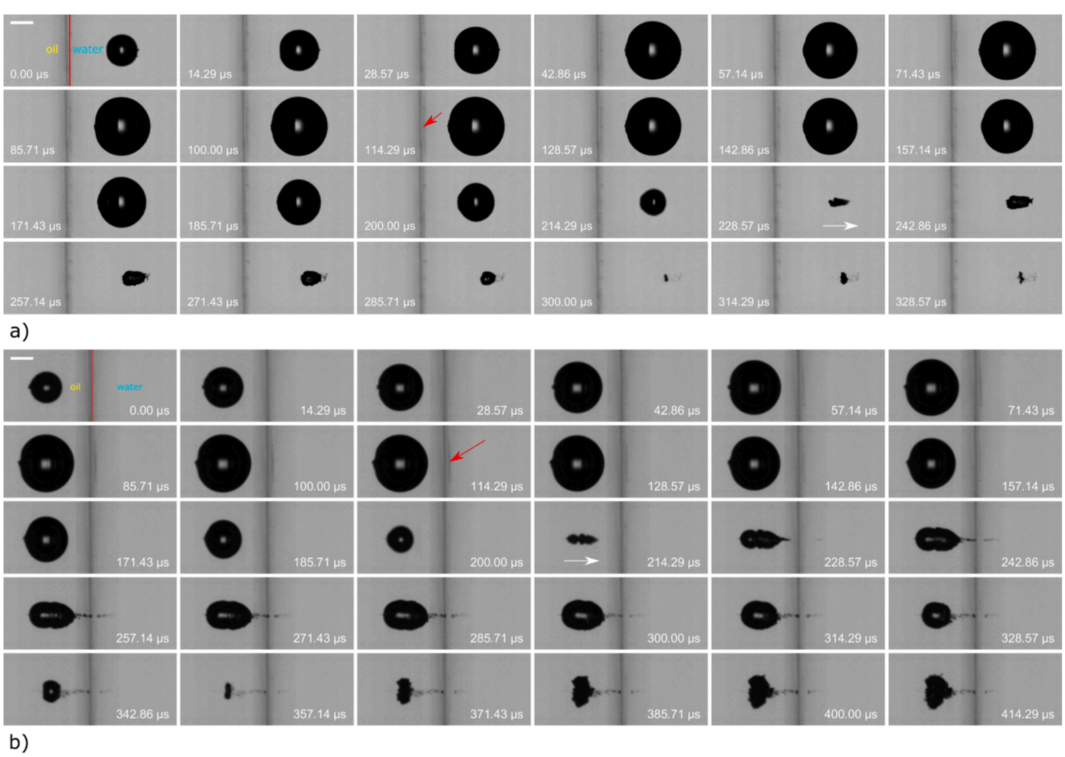

Fig. 2. Recording sequence of cavitation bubble dynamics far from the interface. Bubble is in one case produced in water with $\gamma = 1.78$ ($\zeta = 0.00271$) (a) and in another case in silicone oil with $\gamma = 1.69$ ($\zeta = 0.00301$) (b). The scale bar in the first frame of sequences represents 1 mm. Interface is also marked with a red line in the first frame. Water is on the right side of the interface and silicone oil on the left as noted. White arrow in the frame where jet first appears indicates direction of the jet, red arrow indicates interface bending.

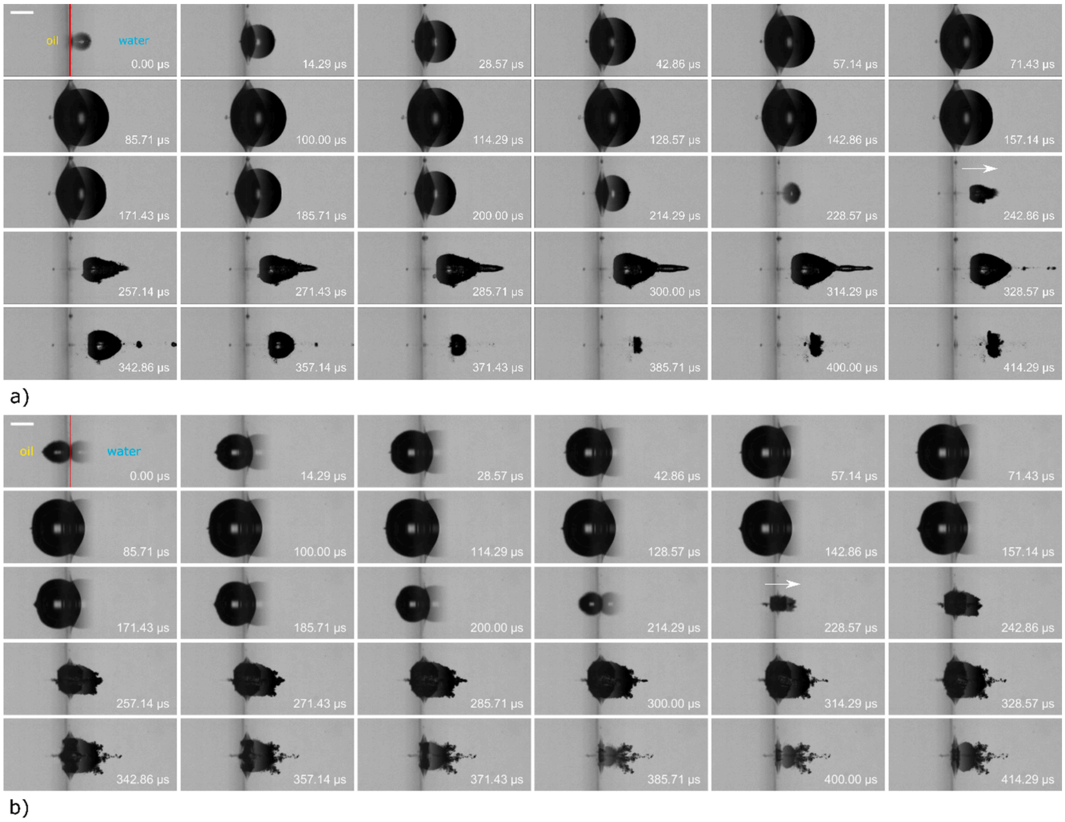

Fig. 3. Recording sequence of cavitation bubble dynamics near the interface. Bubble is in one case produced in water with $\gamma = 0.38$ ($\zeta = 0.0594$) (a) and in another case in silicone oil with $\gamma = 0.44$ ($\zeta = 0.0449$) (b). The scale bar in the first frame of sequences represents 1 mm. Interface is also marked with a red line in the first frame. Water is on the right side of the interface and silicone oil on the left as noted. Arrow in the frame where jet first appears indicates direction of the jet.

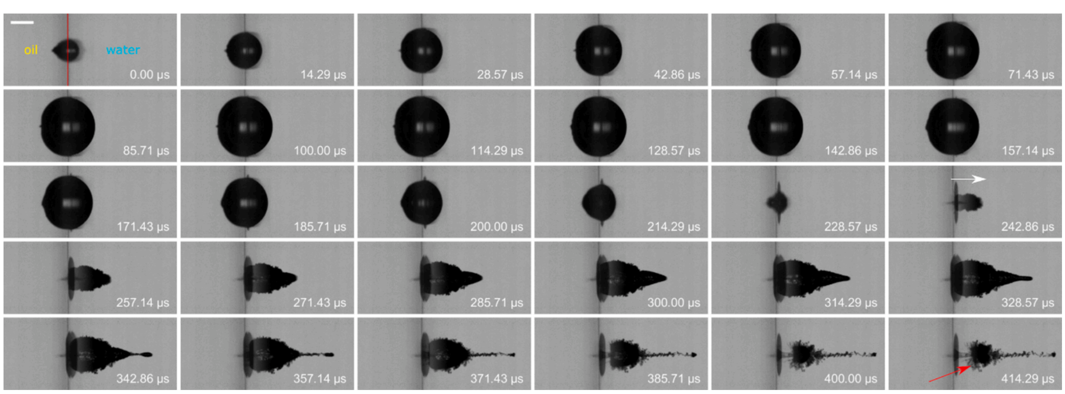

Fig. 4. Recording sequence of cavitation bubble dynamics at the interface with $\gamma \approx 0$ ($\zeta \to \infty$). The scale bar in the first frame of the sequence represents 1 mm. Interface is also marked with a red line in the first frame. Water is on the right side of the interface and silicone oil on the left as noted. White arrow in the frame where jet first appears indicates direction of the jet. Red arrow in the last frame indicates smearing around the bubble by tiny oily droplets.

proximity of the interface, as observed by the noticeably elongated rebounded bubble in Fig. 3a (frames 242.86 µs — 314.29 µs), while in Fig. 3b (frames 228.57 µs — 414.29 µs), the rebounded bubble dynamics gets more complex while it penetrates the interface, implying a more complex jet pattern, although general bubble elongation is still apparent.

Cavitation bubble dynamics at $\gamma \approx 0$ is shown in Fig. 4. Very strong jetting compared to recordings with larger γ coefficient is observed upon bubble collapse, as the bubble is stretching into the water.

A funnel-shaped interface can be noticed in the frames 385.71 µs — 414.29 µs, which is a result of the left part of the bubble being dragged through the interface by the pressure gradient [33], while the bubble surroundings gets smeared with tiny oily droplets around the bubble. The elongated tip of the bubble eventually disintegrates and leaves behind many separate cavitation leftovers concentrated on a line, where the liquid jet flew through. The influence of the interface on bubble dynamics is most pronounced in case of $\gamma \approx 0$, while the interface is not affected much during the bubble growth and collapse phase. The reason that interface appears unaffected is probably that in case of $\gamma \approx 0$, laser-induced plasma appears on both sides of the interface, causing vaporization of both oil and water and thus the interface effectively disappears in the bubble region. The jet however nevertheless appears, since one side of the bubble borders oil and the other side borders water.

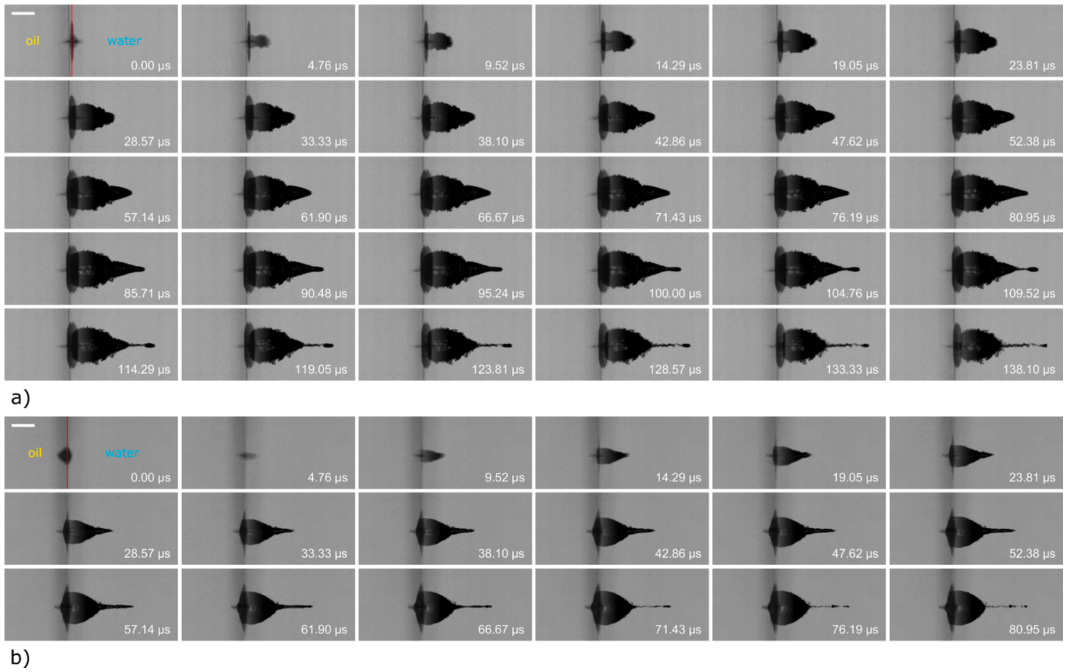

Fig. 5. Recording sequences of jet development in case of interface 1 (a) and interface 2 (b) with $\gamma \approx 0$ ($\zeta \rightarrow \infty$) in both cases. The scale bar in the first frame of sequences represents 1 mm. Interface is also marked with a red line in the first frame. Water is on the right side of the interface and silicone oil on the left as noted. Jet is always directed from left to right.

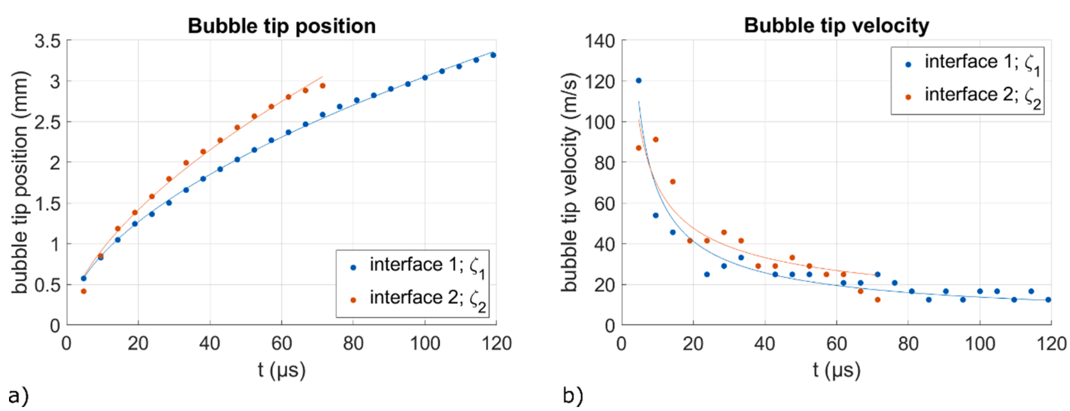

Fig. 6. Propagation of bubble tip position during jetting (a) and velocity of bubble tip during propagation (b). In both cases power function fit was applied.

3.2. *Jet development*

In order to study influence of liquid–liquid interface on a jet-pierced bubble, a comparison between an interface with lower-density silicone oil and water (interface 1) and an interface with higher-density silicone oil and water (interface 2) at $\gamma \approx 0$ was made. Fig. 5a shows cavitation bubble evolution during the liquid jet penetration through the interface 1 while Fig. 5b shows similar evolution in case of interface 2. It takes much longer until the jet-pierced elongated bubble disintegrates. At the same time the elongation of the cavitation bubble is larger in the case of interface 1, indicating a stronger jet. A maximum volume of the cavitation bubble is also larger in the first case (compare frames at 76.19 µs in both cases). All these indications confirm the assertion that effects related to jetting are stronger when difference in densities of liquids on both sides of the interface is larger. Diagram in Fig. 6a shows movement of the tip of the jet-elongated bubble for both cases of the liquid–liquid interface, while diagram in Fig. 6b shows the current velocity of the jet-elongated bubble tip during bubble expansion. Velocity was calculated as a change of tip position between two consecutive frames divided by the time between frames. It can be concluded from the diagrams that in case of interface 1 bubble expands faster in the beginning, but slows down faster and reaches shorter final length before disintegration. In Table 3 jet-elongated bubble characteristics are listed for both discussed cases.

Table 3
Characteristics of jet-elongated bubble.

	Interface 2	Interface 1
Length of jet elongated bubble before disintegration	3.36 mm	3.67 mm
Time from collapse until disintegration	71 µs	119 µs
Maximum bubble volume	1.9 mm^3	2.6 mm^3

3.3. *Different interfaces*

Jet parameters, namely displacement of the bubble center (difference in bubble position at the start of expansion and the end of collapse phase), maximum length of jet-pierced bubble and maximum size of the

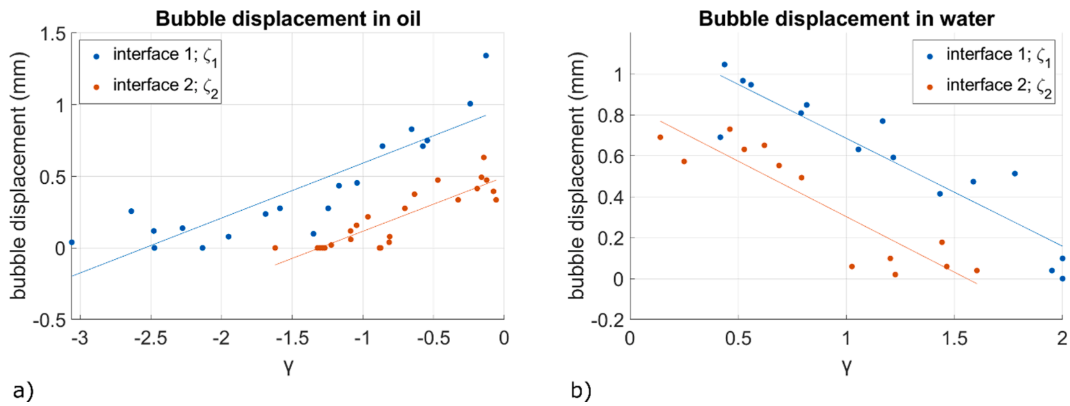

Fig. 7. Bubble displacement in oil (a) and water (b). Linear fit is applied for both cases.

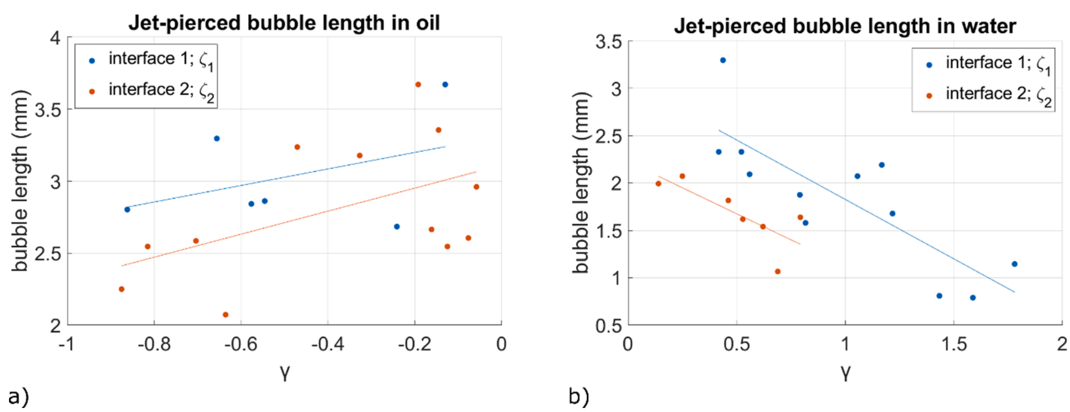

Fig. 8. Maximum length of a jet-pierced bubble in oil (a) and in water (b). The data were fitted with linear function.

rebounded bubble were studied to estimate the influence of the anisotropy parameter on the magnitude of the listed jet parameters. As evident from the Table 1, anisotropy parameter ζ_1 in case of lower-density silicone oil (interface 1) differs by a factor of 2.32 at fixed γ from the case where higher-density silicone oil is used on one side of the liquid–liquid interface (ζ_2 corresponding to interface 2). As will be noticed, the results are quite scattered, which is a result of the statistical nature of the studied phenomena. The shape and size of laser-produced plasma at optical breakdown and thus the exact shape and size of the cavitation bubble varies from pulse to pulse. Small changes in initial conditions lead to significant variance of the secondary effects, i.e. different jet parameters. However, with sufficiently large statistics general trends can be observed and explained by anisotropy parameter.

In Fig. 7 dependence of bubble center displacement on γ coefficient is shown as determined from each recording. Negative γ values represent bubble on the left side of the interface (silicone oil), whereas positive γ values represent bubble produced in water. Throughout the entire range of γ bubble displacement is always larger in case of lower-density silicone oil being used, which is in agreement with the assertion that larger anisotropy parameter results in more intense jet parameters. Moreover, at fixed γ, displacements are approximately two times the size in case of lower-density silicone oil with respect to the higher-density oil, which is almost the same as the ratio between both anisotropy parameters.

Maximum length of a jet-pierced bubble as a function of γ coefficient as measured from recording frames for both types of interfaces is shown in Fig. 8. The elongated bubble is on average longer in the case of lower-density silicone oil being used, however the difference is quite small, especially when bubbles were generated in oil. In the latter case the

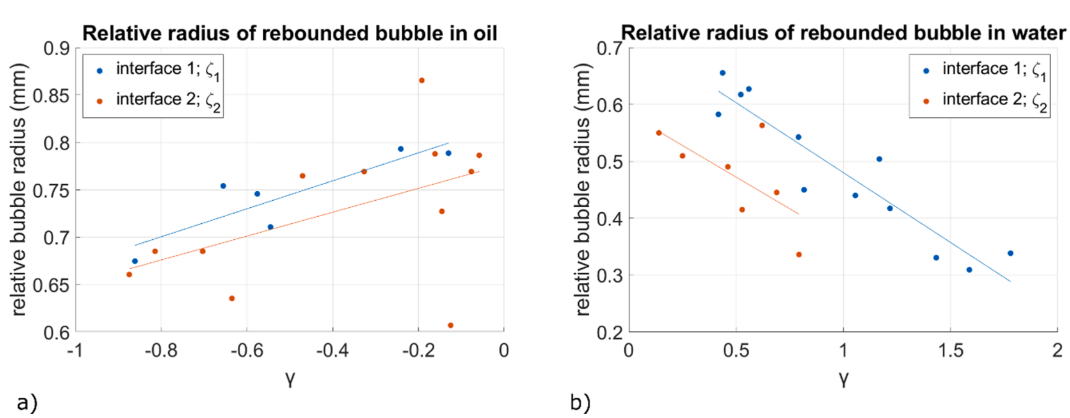

Fig. 9. Maximum relative radius of rebounded bubble in oil (a) and in water (b), measured relatively with respect to the maximum radius of the original bubble.

measurements are scattered throughout the diagram and the difference in general trend of bubble lengths between both types of interfaces can be ascribed to measurement uncertainty. Things are more clear when bubble was generated in water as seen in Fig. 8b, since the behaviour was much more consistent. In general, the measurements agree with the premise of jet parameters being larger in case of larger anisotropy parameter ($\zeta_1 > \zeta_2$), however the difference is not as evident as in the case of bubble displacement.

Lastly, size of the rebounded bubble as measured from the recording frames was compared for both interfaces. Average radius of a rebounded bubble was determined after estimating its maximum volume. Then, relative radius of the rebounded bubble with respect to the maximum radius of the original bubble was calculated at each γ. Similar to previous comparisons maximum size of the rebounded bubble was statistically larger in case of interface with lower-density silicone oil, which is again in correlation with the difference in anisotropy parameter for each surface as seen from the graphs in Fig. 9. Measurements for negative γ values are again much more scattered. Perhaps this can be associated with impurities affecting the measurement consistency.

4. Conclusion

The present paper offers new insights into the interaction between cavitation bubble and a liquid–liquid interface. A flat liquid–liquid interface was achieved, offering a clear view of the details of bubble dynamics near the interface. Extensive measurements were performed in order to cover a vast parameter space of experimental conditions. Two types of liquid–liquid interfaces were used, both consisted of water and silicone oil, however different type of silicone oil was used in each case, one having different density from another. Thus, two sets of experiments were performed, which differed only in anisotropy parameter. According to [27], anisotropy parameter is associated with the magnitude of different observable jet parameters. Three different jet parameters, namely size of rebounded bubble, length of jet-pierced bubble and bubble center displacement were measured for both interfaces. Ratio of magnitudes of observed jet parameters for both interfaces was similar to the ratio of anisotropy parameters corresponding to said interfaces, which is in accordance with the initial preposition. It was observed that bubble center displacement is largest, when the bubble is close to the surface and decreases when bubble is generated further away. In case of larger anisotropy parameter, the displacements are likewise larger. A very similar observation is made for length of jet-pierced bubble and bubble center displacement. Although the measurements were relatively scattered due to statistical nature of studied phenomena, the general trends are readily observed.

Special attention was put on analysis of jet development during bubble collapse for two discussed interfaces. In case where anisotropy parameter was larger, jet propagation took more time and produced longer jet-pierced bubble, although the velocity of bubble tip during jet protrusion was on average larger in case of smaller anisotropy parameter.

CRediT authorship contribution statement

Uroš Orthaber: Investigation, Writing – original draft, Writing – review & editing. **Matevž Dular:** Conceptualization, Visualization, Writing – review & editing, Supervision. **Rok Petkovšek:** Methodology, Supervision, Conceptualization, Writing – review & editing.

Declaration of Competing Interest

The authors declare that they have no known competing financial interests or personal relationships that could have appeared to influence the work reported in this paper.

Acknowledgments

The authors acknowledge the financial support from the Slovenian Research Agency (Core funding No. P2-0270 and P2-0401) and the European Research Council (ERC) under the European Union's Framework Program for research and innovation, Horizon 2020 (grant agreement n 771567 – CABUM).

References

[1] J. Carpenter, M. Badve, S. Rajoriya, S. George, Virendra Kumar Saharan, Aniruddha B. Pandit, Hydrodynamic cavitation: an emerging technology for the intensification of various chemical and physical processes in a chemical process industry, Rev. Chem. Eng. 33 (2017) 433–468, https://doi.org/10.1515/revce-2016-0032.

[2] C.E. Brennen, Cavitation in medicine, Interface Focus. 5 (2015) 20150022, https://doi.org/10.1098/rsfs.2015.0022.

[3] Y. Zhang, X. Xie, Y. Zhang, Y. Zhang, X. Du, Experimental study of influences of a particle on the collapsing dynamics of a laser-induced cavitation bubble near a solid wall, Exp. Therm Fluid Sci. 105 (2019) 289–306, https://doi.org/10.1016/j.expthermflusci.2019.04.005.

[4] W. Xu, Y. Zhai, J. Luo, Q. Zhang, J. Li, Experimental study of the influence of flexible boundaries with different elastic moduli on cavitation bubbles, Exp. Therm Fluid Sci. 109 (2019), 109897, https://doi.org/10.1016/j.expthermflusci.2019.109897.

[5] T.J. Mason, L. Paniwnyk, J.P. Lorimer, The uses of ultrasound in food technology, Ultrason. Sonochem. 3 (1996) S253–S260, https://doi.org/10.1016/S1350-4177(96)00034-X.

[6] E. Riedel, P. Köhler, M. Ahmed, B. Hellmann, I. Horn, S. Scharf, Industrial suitable and digitally recordable application of ultrasound for the enviromentally friendly degassing of aluminium melts before tilt casting, Procedia CIRP. 98 (2021) 589–594, https://doi.org/10.1016/j.procir.2021.01.159.

[7] Y. Xu, H. Cao, Y. Xue, B. Li, W. Cai, Liquid-Phase Exfoliation of Graphene: An Overview on Exfoliation Media, Techniques, and Challenges, Nanomaterials. 8 (2018), https://doi.org/10.3390/nano8110942.

[8] Y.A. Pishchalnikov, O.A. Sapozhnikov, M.R. Bailey, J.C. Williams Jr, R. O. Cleveland, T. Colonius, L.A. Crum, A.P. Evan, J.A. McAteer, Cavitation bubble cluster activity in the breakage of kidney stones by lithotripter shockwaves, J Endourol. 17 (2003) 435–446, https://doi.org/10.1089/089277903769013568.

[9] M. R. Bailey, R. O. Cleveland, T. Colonius, L. A. Crum, A. P. Evan, J. E. Lingeman, J. A. McAteer, O. A. Sapozhnikov, J. C. Williams, Cavitation in shock wave lithotripsy: the critical role of bubble activity in stone breakage and kidney trauma, in: IEEE Symposium on Ultrasonics, 2003, 2003: pp. 724-727 Vol.1. 10.1109/ULTSYM.2003.1293503.

[10] G. Hawlina, D. Perovšek, B. Drnovšek-Olup, J. MoŽina, P. Gregorčič, Optical coherence tomography for an in-vivo study of posterior-capsule-opacification types and their influence on the total-pulse energy required for Nd:YAG capsulotomy: a case series, BMC Ophthalmol. 14 (2014) 131–131. 10.1186/1471-2415-14-131.

[11] A. Vogel, M. Capon, M. Asiyovogel, R. Birngruber, Intraocular Photodisruption with Picosecond and Nanosecond Laser-Pulses - Tissue Effects in Cornea, Lens, and Retina, Invest. Ophthalmol. Vis. Sci. 35 (1994) 3032–3044.

[12] G.L. Chahine, A. Kapahi, J.-K. Choi, C.-T. Hsiao, Modeling of surface cleaning by cavitation bubble dynamics and collapse, Ultrason. Sonochem. 29 (2016) 528–549, https://doi.org/10.1016/j.ultsonch.2015.04.026.

[13] D. Panda, V.K. Saharan, S. Manickam, Controlled Hydrodynamic Cavitation: A Review of Recent Advances and Perspectives for Greener Processing, Processes. 8 (2) (2020) 220.

[14] M. Zupanc, T. Kosjek, M. Petkovšek, M. Dular, B. Kompare, B. Širok, Ž. Blažeka, E. Heath, Removal of pharmaceuticals from wastewater by biological processes, hydrodynamic cavitation and UV treatment, Ultrason. Sonochem. 20 (2013) 1104–1112, https://doi.org/10.1016/j.ultsonch.2012.12.003.

[15] A. Šarc, J. Kosel, D. Stopar, M. Oder, M. Dular, Removal of bacteria Legionella pneumophila, Escherichia coli, and Bacillus subtilis by (super)cavitation, Ultrason. Sonochem. 42 (2018) 228–236, https://doi.org/10.1016/j.ultsonch.2017.11.004.

[16] A. Priyadarshi, M. Khavari, S. Bin Shahrani, T. Subroto, L.A. Yusuf, M. Conte, P. Prentice, K. Pericleous, D. Eskin, I. Tzanakis, In-situ observations and acoustic measurements upon fragmentation of free-floating intermetallics under ultrasonic cavitation in water, Ultrason. Sonochem. 80 (2021), 105820, https://doi.org/10.1016/j.ultsonch.2021.105820.

[17] J.A. Morton, M. Khavari, L. Qin, B.M. Maciejewska, A.V. Tyurnina, N. Grobert, D. G. Eskin, J. Mi, K. Porfyrakis, P. Prentice, I. Tzanakis, New insights into sono-exfoliation mechanisms of graphite: In situ high-speed imaging studies and acoustic measurements, Mater. Today 49 (2021) 10–22, https://doi.org/10.1016/j.mattod.2021.05.005.

[18] T. Stepišnik Perdih, M. Zupanc, M. Dular, Revision of the mechanisms behind oil-water (O/W) emulsion preparation by ultrasound and cavitation, Ultrason. Sonochem. 51 (2019) 298–304, https://doi.org/10.1016/j.ultsonch.2018.10.003.

[19] W.H. Wu, D.G. Eskin, A. Priyadarshi, T. Subroto, I. Tzanakis, W. Zhai, New insights into the mechanisms of ultrasonic emulsification in the oil–water system and the role of gas bubbles, Ultrason. Sonochem. 73 (2021), 105501, https://doi.org/10.1016/j.ultsonch.2021.105501.

[20] M. Dular, T. Požar, J. Zevnik, R. Petkovšek, High speed observation of damage created by a collapse of a single cavitation bubble, Wear 418–419 (2019) 13–23, https://doi.org/10.1016/j.wear.2018.11.004.
[21] M. Hosbach, R. Skoda, T. Sander, U. Leuteritz, M. Pfitzner, On the temperature influence on cavitation erosion in micro-channels, Exp. Therm Fluid Sci. 117 (2020), 110140, https://doi.org/10.1016/j.expthermflusci.2020.110140.
[22] M. Hosbach, S. Gitau, T. Sander, U. Leuteritz, M. Pfitzner, Effect of taper, pressure and temperature on cavitation extent and dynamics in micro-channels, Exp. Therm Fluid Sci. 108 (2019) 25–38, https://doi.org/10.1016/j.expthermflusci.2019.05.012.
[23] I. Tzanakis, L. Bolzoni, D.G. Eskin, M. Hadfield, Evaluation of Cavitation Erosion Behavior of Commercial Steel Grades Used in the Design of Fluid Machinery, Metallurgical and Materials Transactions A. 48 (2017) 2193–2206, https://doi.org/10.1007/s11661-017-4004-2.
[24] G.L. Chahine, A. Bovis, Oscillation and Collapse of a Cavitation Bubble in the Vicinity of a Two-Liquid Interface, in: W. Lauterborn (Ed.), Cavitation and Inhomogeneities in Underwater Acoustics, Springer Berlin Heidelberg, Berlin, Heidelberg, 1980, pp. 23–29.
[25] U. Orthaber, J. Zevnik, R. Petkovšek, M. Dular, Cavitation bubble collapse in a vicinity of a liquid-liquid interface – Basic research into emulsification process, Ultrason. Sonochem. 68 (2020), 105224, https://doi.org/10.1016/j.ultsonch.2020.105224.
[26] P.-H. Tsai, T. Kurniawan, A.-B. Wang, A simple technique to achieve meniscus-free interfaces, Phys. Fluids 31 (2019), 011702, https://doi.org/10.1063/1.5080659.
[27] O. Supponen, D. Obreschkow, M. Tinguely, P. Kobel, N. Dorsaz, M. Farhat, Scaling laws for jets of single cavitation bubbles, J. Fluid Mech. 802 (2016) 263–293, https://doi.org/10.1017/jfm.2016.463.
[28] Yu.L. Levkovskii, V.P. Il'in, Effect of surface tension and viscosity on the collapse of a cavitation bubble, J. Eng. Phys. 14 (1968) 478–480. 10.1007/BF00828072.
[29] H. Nazari-Mahroo, K. Pasandideh, H.A. Navid, R. Sadighi-Bonabi, How important is the liquid bulk viscosity effect on the dynamics of a single cavitation bubble? Ultrason. Sonochem. 49 (2018) 47–52, https://doi.org/10.1016/j.ultsonch.2018.07.013.
[30] J.-P. Franc, The Rayleigh-Plesset equation: a simple and powerful tool to understand various aspects of cavitation, in: L. d'Agostino, M.V. Salvetti (Eds.), Fluid Dynamics of Cavitation and Cavitating Turbopumps, Springer Vienna, Vienna, 2007: pp. 1–41. 10.1007/978-3-211-76669-9_1.
[31] I. Tzanakis, G.S.B. Lebon, D.G. Eskin, K.A. Pericleous, Characterizing the cavitation development and acoustic spectrum in various liquids, Ultrason. Sonochem. 34 (2017) 651–662, https://doi.org/10.1016/j.ultsonch.2016.06.034.
[32] I. Tzanakis, M. Hadfield, I. Henshaw, Observations of acoustically generated cavitation bubbles within typical fluids applied to a scroll expander lubrication system, Exp. Therm. Fluid Sci. 35 (2011) 1544–1554, https://doi.org/10.1016/j.expthermflusci.2011.07.005.
[33] S. Cleve, C. Inserra, P. Prentice, Contrast Agent Microbubble Jetting during Initial Interaction with 200-kHz Focused Ultrasound, Ultrasound Med. Biol. 45 (2019) 3075–3080, https://doi.org/10.1016/j.ultrasmedbio.2019.08.005.